Geophysical Research Letters

RESEARCH LETTER
10.1029/2024GL108798

Key Points:

- Internal variability has enhanced Arctic warming but suppressed global warming over 1980–2022
- This manifestation of internal variability is rare in model simulations but has a robust global surface air temperature (SAT) trend pattern
- This internal SAT pattern features warming in the Barents and Kara Sea and cooling of the Tropical Eastern Pacific and Southern Ocean

Supporting Information:

Supporting Information may be found in the online version of this article.

Correspondence to:

A. J. Sweeney and Q. Fu,
aodhan@uw.edu;
qfu@uw.edu

Citation:

Sweeney, A. J., Fu, Q., Po-Chedley, S., Wang, H., & Wang, M. (2024). Unique temperature trend pattern associated with internally driven global cooling and Arctic warming during 1980–2022. *Geophysical Research Letters*, *51*, e2024GL108798. https://doi.org/10.1029/2024GL108798

Received 10 FEB 2024
Accepted 8 MAY 2024

Unique Temperature Trend Pattern Associated With Internally Driven Global Cooling and Arctic Warming During 1980–2022

Aodhan J. Sweeney[1], Qiang Fu[1], Stephen Po-Chedley[2], Hailong Wang[3], and Muyin Wang[4,5]

[1]Department of Atmospheric Sciences, University of Washington, Seattle, WA, USA, [2]Lawrence Livermore National Laboratory, Program for Climate Model Diagnosis and Intercomparison, Livermore, CA, USA, [3]Atmospheric, Climate, and Earth Sciences Division, PNNL, Richland, WA, USA, [4]Cooperative Institute for Climate, Ocean, and Ecosystem Studies, University of Washington, Seattle, WA, USA, [5]Pacific Marine Environmental Laboratory, Oceanic and Atmospheric Research, NOAA, Seattle, WA, USA

Abstract Diagnosing the role of internal variability over recent decades is critically important for both model validation and projections of future warming. Recent research suggests that for 1980–2022 internal variability manifested as Global Cooling and Arctic Warming (i-GCAW), leading to enhanced Arctic Amplification (AA), and suppressed global warming over this period. Here we show that such an i-GCAW is rare in CMIP6 large ensembles, but simulations that do produce similar i-GCAW exhibit a unique and robust internally driven global surface air temperature (SAT) trend pattern. This unique SAT trend pattern features enhanced warming in the Barents and Kara Sea and cooling in the Tropical Eastern Pacific and Southern Ocean. Given that these features are imprinted in the observed record over recent decades, this work suggests that internal variability makes a crucial contribution to the discrepancy between observations and model-simulated forced SAT trend patterns.

Plain Language Summary When comparing model simulations of Earth's recent warming to real-world observations, differences may arise from several factors. Two important factors are the model errors in the simulated response to increased greenhouse gases, and natural fluctuations within the climate system that produced discrepancies between observations and models. Thus, quantifying the role of these natural fluctuations is important for the assessment of model-observation differences. Previous studies have shown that natural climate variability has depressed global warming and enhanced Arctic warming. By compositing the multi-decadal trend patterns from CMIP6 simulations in which natural variability warms the Arctic but has a global cooling effect, we find that the majority of these model simulations also produce enhanced warming in the Barents and Kara Seas and cooling in the Tropical Eastern Pacific and Southern Ocean due to natural variability. Since these are the exact features imprinted on observed surface temperature changes over 1980–2022, our work suggests that natural variability is an important component of several noteworthy differences between models and observations.

1. Introduction

Global surface air temperatures (SAT) since 1980 have experienced significant warming due to increased greenhouse gas concentrations and reduced aerosols (IPCC, 2023). Yet, the pattern of the observed warming has larger spatial variability than the warming simulated by climate models (e.g., Hansen et al., 2010). One of the most prominent features of both observed and simulated warming is Arctic Amplification (AA): a ratio of Arctic to global SAT trend larger than one (Manabe & Wetherald, 1975). From 1980 to 2022 observed SAT in the Arctic (defined as poleward of 70°N) warmed over four times faster than the global mean, leading to an AA of 4.2 (Rantanen et al., 2022). Although models simulate greater Arctic warming relative to the global mean, the observed values of AA over 1980 to 2022 are larger than AAs from 94% of historical simulations from large ensembles in the Coupled Model Intercomparison Project Phase 6 (CMIP6) (Chylek et al., 2022, 2023, 2024; Hahn et al., 2021; Rantanen et al., 2022; Sweeney et al., 2023; Ye & Messori, 2021). The discrepancy between the model predicted AA and that observed from 1980 to 2022 may be due to a model bias in the forced response of the Arctic and/or global climate, leading to concerns regarding model fidelity (Chylek et al., 2022; Rosenblum & Eisenman, 2017). Another potential cause of this discrepancy is a rare configuration of internal climate variability

in the last four decades (Chylek et al., 2023; Deser et al., 2012a, 2012b; Feng et al., 2021; Kay et al., 2011; Zhou et al., 2024). Key to reconciling this model-observation discrepancy is separating the forced response from internal variability (e.g., Lehner & Deser, 2023).

Various methodologies have been proposed to partition the forced and internal components of climate change (e.g., Barnes et al., 2019; Dai et al., 2015; Deser et al., 2014; Foster & Rahmstorf, 2011; Gordon et al., 2021; Labe & Barnes, 2022; Po-Chedley et al., 2022; Rader et al., 2022; Räisänen, 2021; Sippel et al., 2021; Wallace et al., 2012). Pattern recognition algorithms have shown promise with this task (Wills et al., 2020), because the SAT response to external forcing is more spatially uniform than the more complex patterns associated with internal variability. The patterns of the forced response and internal variability can be differentiated in large ensembles, which contain many simulations of the Earth's climate with varying initial conditions and then produce unique manifestations of the internal variability (and thus unique patterns of warming) (Deser et al., 2020; Kay et al., 2015). Large ensembles therefore provide a useful training data set for pattern recognition algorithms designed to distinguish between the forced and unforced climate response. Recently, Sweeney et al. (2023) (referred to herein as S2023) showed that the pattern recognition algorithms based on machine learning can help partition the role of internal variability and the forced response to better understand the model-observation discrepancy in AA from 1980 to 2022. Their results indicate that internal variability has enhanced AA for 1980–2022 by 38%. After removing the contribution of internal variability from the observations, they can reconcile differences between simulated and observed AA.

The identified manifestation of internal variability that creates the exceptionally high value of observed AA features internally driven global-cooling and Arctic-warming (referred to hereafter as i-GCAW). When this i-GCAW is imprinted onto the Earth's warming due to external forcing, the effect is to enhance the rate of Arctic warming while damping the global mean warming trend during 1980–2022. A number of studies have suggested that internal variability has warmed the Arctic and cooled the globe in the last few decades, evidenced by rapid sea ice concentration decline (e.g., Ding et al., 2019) and a lack of warming (or even cooling) in the Tropical Eastern Pacific and Southern Ocean (e.g., Feng et al., 2021; Kosaka & Xie, 2013; Po-Chedley et al., 2021; J. H. L. Zhang et al., 2019, L. Zhang et al., 2019). These studies reinforce the result from S2023 that internal variability produced global-cooling and Arctic-warming during 1980–2022.

This study aims to investigate model simulations that have an imprint of i-GCAW. These simulations can provide insight into the global internally driven trend pattern since 1980. It thus has value for understanding model-observation discrepancies and may help constrain uncertainty in future patterns of SAT change (Lehner & Deser, 2023). Here we first show that the observationally derived i-GCAW in S2023 occurs rarely in the ensemble members from various models and confirm that the machine learning algorithms developed in S2023 have minimal biases when applied to this subset of rare ensemble members. We then show that the ensemble members featuring similar i-GCAW to observationally derived values share a preferred internally driven global SAT trend pattern, including warming in the Barents and Kara Sea and cooling in the Tropical Eastern Pacific and Southern Ocean. We further examine the pattern of differences between the observed SAT trend pattern and the forced warming pattern derived from the CMIP6 multi-model mean scaled by observationally derived forced global-mean SAT trend in S2023. The difference trend pattern—which represents an estimate of the impact of internal variability on the pattern of satellite era SAT trends—also shows warming in the Kara Sea and cooling of the Tropical Eastern Pacific and Southern Ocean. Both approaches indicate a common imprint of internal variability on the pattern of surface warming during recent decades. Finally, we examine the evolution of AA over the ensuing 20 years in the ensemble members that exhibit i-GCAW over a 43-year period (matching the length of the observational record from 1980 to 2022). These simulations suggest a decrease of the mean AA from 4.2 to 3.4, supporting the claim in S2023 that the exceptional AA over 1980 to present will not persist into the future.

2. Data

Data used here is largely the same as from S2023. The model simulations come from large ensembles included in CMIP6 using 10 different models that contain 10 to 50 ensemble members. Aside from the CMIP6 models, we also include the CESM2 large ensemble with updated biomass burning aerosol emissions (Fasullo et al., 2022; Rodgers et al., 2021), as well as the E3SM2 large ensemble (Fasullo et al., 2024). SAT trend maps are calculated by finding the ordinary least-squares regression at each grid point using 43-year periods (the duration of the satellite era from 1980 to 2022) separated by five years spanning 1850–2047 (i.e., 1850–1892, 1855–1897, …,

1980–2022, …, 2005–2047). Historical simulations for the large ensembles end in 2014. For those models where more than 10 ensemble members have data through 2047 using the Shared Socioeconomic Pathways 3 or 5 (SSP3-7.0 or SSP5-8.5), the simulations are extended (using SSP5-8.5 when both are available) (O'Neill et al., 2016). Of the 12 large ensembles used, 8 have extensions past the 2014 period, while 4 end in 2014 (see Table S1 in Supporting Information S1 for information regarding the large ensembles). For each of the 12 models, we compute the area average (global and Arctic) trends for each ensemble member, and the internal trends are the difference between these trends and forced trends that are computed by taking the ensemble average across all ensemble members.

Observational SAT trends shown here are the average of four datasets, including the Met Office Hadley Centre/Climate Research Unit's global surface temperature dataset version 5, Berkeley Earth Land/Ocean Temperature Record, GISS Surface Temperature Analysis version 4, and the NOAA Merged Land Ocean Global Surface Temperature Analysis version 5 (Lenssen et al., 2019; Morice et al., 2021; Rohde & Hausfather, 2020; J. H. L. Zhang et al., 2019, L. Zhang et al., 2019). All SAT trend maps are regridded to a common 2.5° × 2.5° latitude-by-longitude grid.

We also use Pre-Industrial Control (piControl) simulations from the 10 CMIP6 models used above, which allows for investigation of simulated internal variability without the role of forcings (Eyring et al., 2016). Internal variability is identified using 43-year trends separated by five years for all available ensemble members given that the ensemble member has at least 100 available years in the piControl simulation.

3. Internally Generated Global-Cooling and Arctic-Warming

Quantifying the internal component of recent SAT trends remains a crucial problem in climate science (Schlesinger & Ramankutty, 1994; Watanabe et al., 2021; Wills et al., 2022; Xie & Kosaka, 2017). In this section, we show that a robust pattern of internal variability can be obtained by compositing model simulations with i-GCAW similar to observationally derived values. S2023 estimated that between 1980 and 2022, internal variability reduced observed global warming by −0.024 K/dec and enhanced Arctic warming by 0.145 K/dec. Across all 43-year SAT trends from the large ensembles between 1850 and 2047, the standard deviation of internally generated SAT trends over the globe and in the Arctic are 0.025 K/dec and 0.157 K/dec, respectively. Thus, when viewed individually, the observationally inferred estimates of internal variability are about one standard deviation from the mean (zero), and thus not rare.

Given that internal variability both enhanced Arctic warming and depressed global warming, it is useful to examine the frequency of these events concurrently. Figure 1 shows the Arctic versus global mean internal trends for 43 years from all large ensembles over 1850–2047, indicating that Arctic and global internal trends are positively correlated in model simulations ($r = 0.72$). While many studies have examined the coupling between global and Arctic temperature as a response to forced climate change, internal variability is also important for the coupling of global and Arctic temperature (Screen & Deser, 2019). The thick red line in Figure 1 shows that the ordinary least-squares fit of Arctic to global internal trends has a slope of 4.46, meaning that an internally driven change in global SAT is typically amplified by a factor of 4.46 in the Arctic. This is analogous to Arctic Amplification but operating through multidecadal internal variability alone. 74% of all simulated 43-year trends are confined to quadrants I and III (top-right and bottom-left) in Figure 1, where Arctic and global internal variability have the same sign. Only 26% of simulations exist in quadrants II and IV (top-left and bottom-right), where the Arctic and global internal trends have opposing signs. The observationally inferred trends of internal variability from S2023 sits in quadrant II, a sparsely populated region. The observational estimate is near the edge of the distribution suggesting that Earth may have experienced a rare configuration of internal variability over 1980–2022.

To gain confidence in the observational estimate in Figure 1, we apply the ML algorithm trained in Sweeney et al. (2023) to the subset of 43-year trends which occur during 1980–2022 and are in quadrant II. The mean estimated forced AA for these cases is 2.92 based on the S2023 ML algorithm, versus the mean true forced AA of 2.72. The latter is based on the forced AA from the corresponding ensemble mean. That the ML derived forced AA is similar to the true forced AA suggests that the algorithm used in S2023 to estimate the role of global and Arctic internal variability can do so accurately in model simulations, even when those simulations occur with rare configurations of internal variability like the i-GCAW. This provides confidence that the estimated effects of internal variability are accurate.

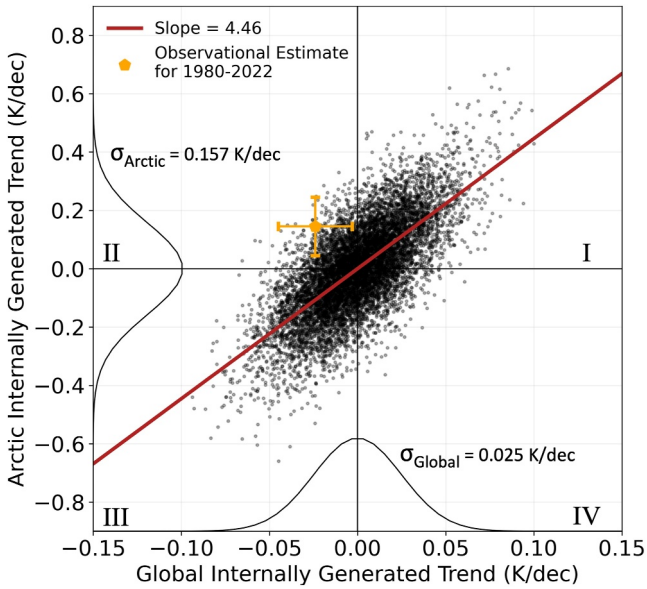

Figure 1. Arctic versus global internal trends from all large ensembles between 1850 and 2047. Each gray circle represents an internal trend from one ensemble member over one 43-year period. Thin black lines show the normalized probability density functions of all global and Arctic internal trends with the corresponding standard deviations provided. The orange pentagon shows the observationally derived internal trends for 1980–2022 with one-standard deviation error bars from S2023. The red line shows the ordinary-least squares regression of the Arctic internal trend onto that of the global internal trend, which has a slope of 4.46 and a correlation coefficient of 0.72. Roman numerals denote the quadrant number.

The observationally inferred estimate suggests that from 1980 to 2022 the Earth experienced i-GCAW. However, it does not provide information on the accompanying spatial pattern of the SAT trends. To investigate the SAT trend pattern associated with i-GCAW, we select 43-year trends in quadrant II with internally generated global cooling and Arctic warming magnitudes larger than $\sigma_{Global}/2$ and $\sigma_{Arctic}/2$, respectively (Figure 1). We note that this threshold of i-GCAW is less than the observational estimate in Figure 1 but is a lower limit. It is also chosen to make sure that there are enough samples in the subset. This subset contains 154 samples out of a total 9,121 points in Figure 1. These i-GCAW cases are thus a rare configuration of internal variability. These selected simulations show no obvious propensity for onset between 1850 and 2047, nor are these cases limited to a small subset of climate models (see Figure S1 and Table S1 in Supporting Information S1). Figure 2 shows the global internal SAT trend pattern created by averaging over the 154 i-GCAW cases at each grid point. We reproduced Figures 1 and 2 but using the CMIP6 piControl simulations (Figures S2 and S3 in Supporting Information S1), showing almost identical results (comparing Figures S2 and S3 in Supporting Information S1 with Figures 1 and 2). We also produced average trend maps using the same thresholds for quadrant I (internal Global Warming and Arctic Warming; i-GWAW), quadrant III (internal Global Cooling and Arctic Cooling; i-GCAC), and quadrant IV (internal Global Warming Arctic Cooling; i-GWAC), which are provided in Figure S4 in Supporting Information S1.

The SAT trend pattern shown in Figure 2 is derived entirely from model simulated internal variability based on simulations exhibiting internally generated global cooling and Arctic warming. The results suggest that i-GCAW has a preferred internal SAT trend pattern, which is unique compared to other configurations of internal variability shown in Figure S4 in Supporting Information S1. Notable warming is featured in the Barents and Kara Sea relative to other locations in the Arctic, while cooling is evident throughout the Tropical Eastern Pacific in addition to continental cooling in northern South America, central Africa, and parts of central Asia. A region of strong cooling is also located in the

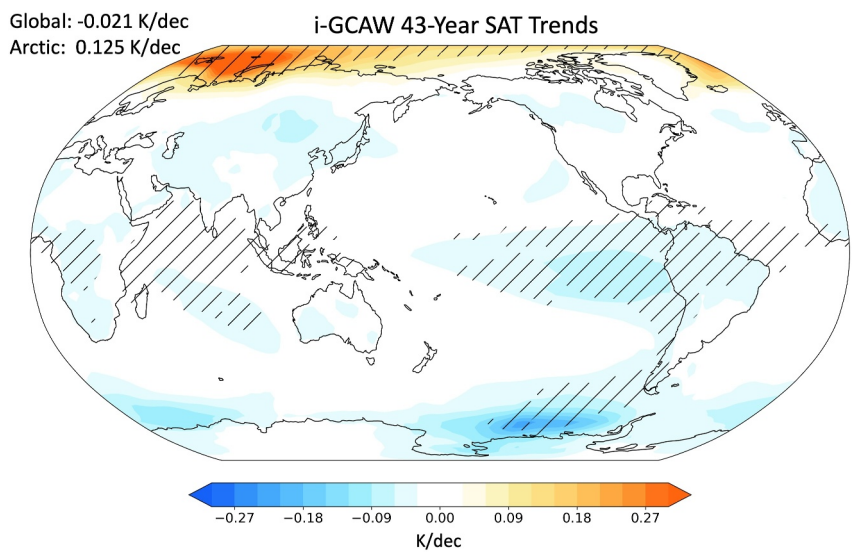

Figure 2. The 43-year SAT trend pattern due to internal variability obtained by averaging over 154 cases which have internally driven global cooling and Arctic warming (i-GCAW) magnitudes larger than $\sigma_{Global}/2$ and $\sigma_{Arctic}/2$ (see Figure 1), respectively. Hatching represents the regions where over 80% of the cases agree on sign. The domain averaged Arctic and global mean temperature trends are provided on the top left.

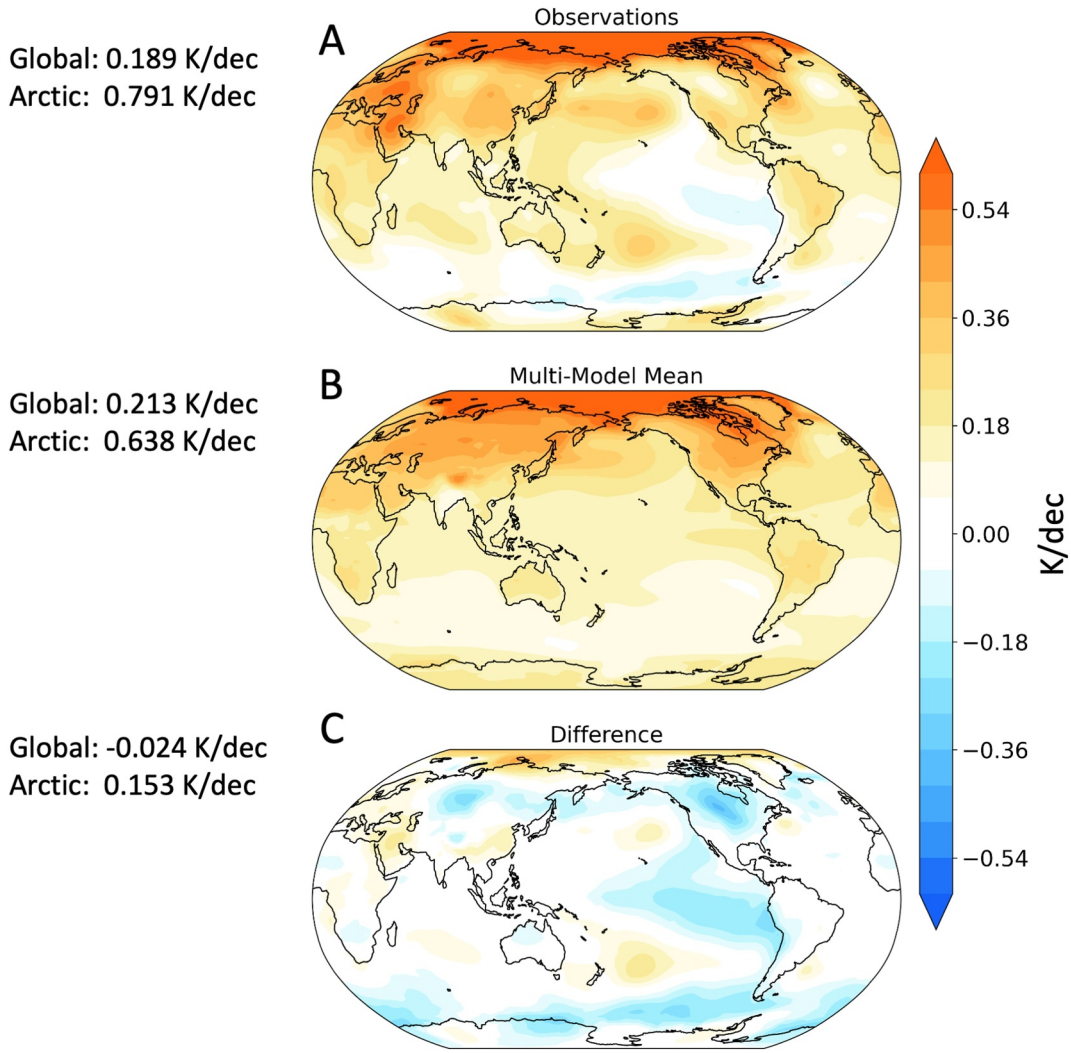

Figure 3. The SAT trend pattern from 1980 to 2022 in (a) observations, (b) the multi-model mean (MMM) forced trend scaled by observationally derived global mean forced trend from S2023, and (c) the difference between (a) and (b). Observations are the mean over four observational data sets (see Section 2), and the MMM is the average forced trend scaled so that the global mean warming is equal to 0.213 K/dec (see text).

Amundsen Sea, linking tropical cooling of the Eastern Pacific to the Southern Ocean (Ding & Steig, 2013; Dong et al., 2022; Hwang et al., 2017; Stuecker et al., 2017). Interestingly, many of these features are sufficiently strong that they are imprinted onto the observed warming pattern (shown in Figure 3a); namely, enhanced Barents and Kara Sea warming, Eastern Pacific cooling, and Southern Ocean cooling. Figure S4 in Supporting Information S1 shows that the average trend map for i-GWAC (quadrant IV) is essentially the mirror of i-GCAW. While both i-GCAW and i-GWAC patterns have global features agreed upon by over 80% of ensemble members (signified by hatching in Figure 2), the average i-GWAW and i-GCAC (quadrants I and III) trend maps are focused on the Northern Hemisphere, and do not share consistent global features (see Figure S4 in Supporting Information S1). Note that the trend pattern in Figure 2 has a mean Arctic warming of 0.125 K/dec and global cooling of −0.021 K/dec, which are roughly 15% weaker than those from the observational estimates in S2023. Using more stringent criterion with global cooling and Arctic warming magnitudes larger than $\frac{3}{4}\sigma_{\text{Global}}$ and $\frac{3}{4}\sigma_{\text{Arctic}}$, similar but stronger features are shown (see Figure S5 in Supporting Information S1).

The forced SAT trend pattern over 1980–2022 can be obtained from the multi-model mean (MMM) from 8 models that cover this period (Table S1 in Supporting Information S1). This MMM, however, may have biases due to errors in climate sensitivity and radiative forcings (Tokarska et al., 2020; IPCC chapter 4, 2023). Here we

attempt to minimize the impact of these biases by scaling the MMM trend pattern with the observationally estimated forced global trend of 0.213 K/dec for 1980–2022 (S2023). A rough estimate of the global internal trend pattern for 1980–2022 can then be obtained as the difference between observed trends and the scaled MMM trend. Figure 3 shows the SAT trend patterns for 1980–2022 from (A) observations, (B) the scaled MMM, and (C) the difference between A and B. While scaling gives us more confidence in the magnitude of the forced trend, it does not change the trend pattern. If the scaled MMM correctly captures the forced pattern of climate change, then the difference in panel C represents the internal trend contribution to the observational record. On the other hand, biases in the simulated forced pattern of warming would produce errors in this estimate of the impact of internal variability.

Observations show many features in the SAT trends not seen in the MMM. While the scaled MMM suggests that external forcing should have produced weak warming throughout the Tropical Eastern Pacific and Southern Ocean from 1980 to 2022, observations exhibit weak cooling in these regions. The difference panel in Figure 3c shows Arctic warming and cooling in the Tropical Eastern Pacific that connects to extensive cooling of the Southern Ocean and is strongest in the Amundsen Sea. Figure 3c also shows cooling in the northern hemisphere extratropical continents. Notably, many of the features present in the difference pattern of Figure 3c are also seen in the climate model composite of the i-GCAW shown in Figure 2. Both figures show warming around the Kara Sea, and cooling throughout the Tropical Eastern Pacific and Southern Ocean. The area weighted spatial correlation between the composite trend pattern in Figure 2 and the difference pattern in Figure 3c is $r = 0.5$, which may be surprising given that the trend pattern in Figure 2 is based on model simulated internal variability preconditioned only on i-GCAW. The similarity of the global trend patterns from the two methods that are constrained by observations in very different ways strongly suggests that the trend pattern shown in Figure 3c is largely impacted by the trend pattern of internal variability in the last few decades.

The analysis shown here suggests that from 1980 to 2022 internal variability manifested as an i-GCAW, a rare configuration of internal variability in model simulations. This configuration of internal variability exhibits a unique but robust SAT trend pattern, agreed upon by simulations from different models and over different time periods. The i-GCAW pattern main features are also visible in the differences between the observations and the scaled MMM, suggesting that the pattern associated with i-GCAW is imprinted onto the observed SAT trend pattern from 1980 to 2022. This also suggests that a plausible trend pattern of internal variability can be obtained by solely restricting simulations based on i-GCAW. We next evaluate the implications of this finding and attempt to predict the future evolution of internal variability.

3.1. Implications for Future Arctic Amplification

Figure 2 showed that i-GCAW has a robust spatial pattern, with several regions showing strong model agreement. If models also agree on the SAT evolution after a given i-GCAW period considered (i.e., 43 years), it may then be possible to predict the future evolution of SAT trends. In this section, we attempt to use the simulated i-GCAW cases to predict the future evolution of the internal variability and evaluate its implications for AA.

To do this, we take all 154 cases of i-GCAW used to compose Figure 2 and evaluate the SAT trend evolution over the subsequent 20-year after the i-GCAW was identified. These evolutions of the simulated internal variability are referred to as trajectories and are used to evaluate the potential evolution from the recent observed instance of i-GCAW. Because we only use data from 1850 to 2047, 22 of the 154 i-GCAW cases are identified after the period of 1990–2032 and do not have the full 20-year trajectories available. In these cases we use the abbreviated trajectory, for example, if an i-GCAW case is identified over 2000–2042 we just use the trajectory for the following five years. Figure 4a shows the predicted SAT trend patterns after extending the i-GCAW trajectories by 5, 10, 15, and 20 years. We also show 5-, 10-, 15-, and 20-year SAT trend patterns following identification of an i-GCAW in Figure S6 in Supporting Information S1. Results of Figure 4a suggest that while cooling trends in the Tropical Eastern Pacific degrade after the first decade, the Amundsen Sea cooling trend remains a persistent feature with over 80% of trajectories agreeing on this cooling even when trends are calculated with another 20 years of data. While the trajectories suggest that internally generated Arctic warming will persist in future trend calculations, this signal loses its significance during the second decade of projections. Figure S7 in Supporting Information S1 shows a recreation of Figure 4 but using 43-year trends at 5, 10, 15, and 20 years after the initial i-GCAW is identified (i.e., the 43-year window is shifted by 5, 10, 15, and 20 years to recalculate the internally generated trend). Results of Figures S6 and S7 in Supporting Information S1 indicate that the degradation of

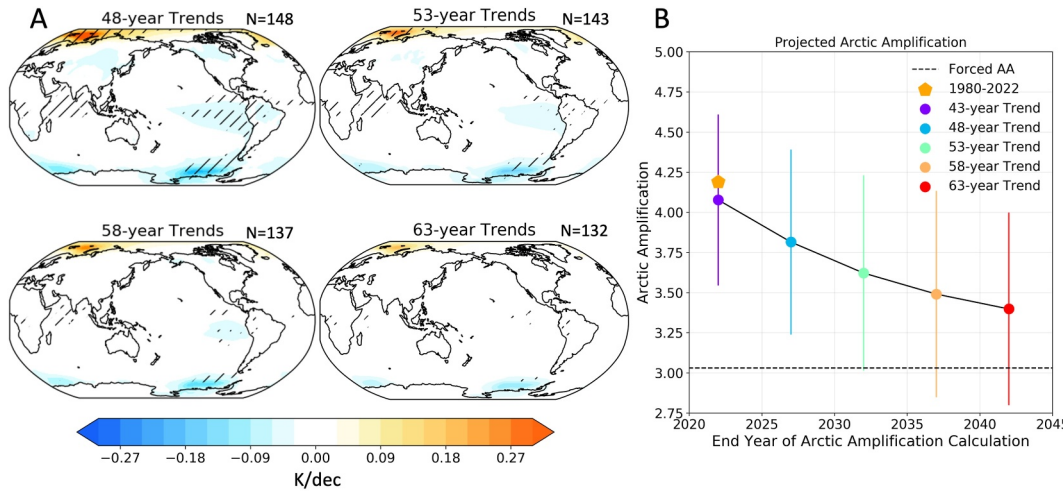

Figure 4. (a) Internally generated SAT trends extended by 5, 10, 15, and 20 years after the i-GCAW pattern has been identified. Hatching indicates regions where over 80% of the cases agree on sign. The number of samples (N) used in the composite of each trend map is shown in the top right. (b) Impact of predicted future configurations of internal variability for Arctic Amplification (AA). Colored dots show model derived AA values given the forced trend (dashed line) from S2023. The orange pentagon shows the AA during the 1980–2022 period from observations. Error bars show the two-sigma confidence interval of future AA using all available trajectories. The black dashed line shows the estimate of the forced AA ratio (3.03) over 1980–2022 from S2023.

significance in the Arctic signal shown in Figure 4a is due to strong internally driven cooling in the Arctic after i-GCAW episodes.

Figure 4b shows the future values of AA based on the trajectories of the i-GCAW. The observed AA (shown in orange pentagon) during the 1980–2022 period is inflated above the dashed black line due to internal variability. Based on the mean evolution of the internal trend pattern associated with i-GCAW in Figure 4a, future values of AA are shown as colored points in Figure 4b. Given that each realization of i-GCAW in model simulations may have different magnitudes of global-cooling and/or Arctic-warming when identified, all trajectories are computed relative to their initial magnitudes. While on average the AA metric tends to relax toward the forced trend as the length of time used for the AA calculation increases, the model trajectories indicate that elevated values of AA may persist into the 2040s (England et al., 2015). Figure 4b suggests that the rare configuration of internal variability that produced large observed values of AA will moderate and AA will subside over the next two decades.

4. Discussion and Conclusions

The observationally inferred trend of internal variability from 1980 to 2022 suggests global cooling and Arctic warming. Model simulations infrequently simulate this observationally derived variability, suggesting that the Earth experienced a rare configuration of internal variability from 1980 to 2022. To investigate the spatial pattern of SAT trends associated with the i-GCAW, large ensemble simulations were used to identify cases with the i-GCAW. The spatial SAT trend pattern associated with the i-GCAW is unique, spanning the globe with many robust features, which are distinct from other multi-decadal internal SAT trend patterns (see Figure S4 in Supporting Information S1). These unique and robust features associated with the i-GCAW are also imprinted on the observational record, providing strong evidence that the Earth indeed experienced the i-GCAW from 1980 to 2022.

Whether discrepancies between climate models and observations are due to a rare configuration of internal variability or model biases in the forced response is a crucial issue in climate science. Of particular importance are the observed cooling trends in the Tropical Eastern Pacific over recent decades. These cooling trends generally disagree with simulations which predict a warming response (e.g., Seager et al., 2019; Seager et al., 2022). Due to the myriad of teleconnections between this region and higher latitudes (e.g., Baxter et al., 2019; Trenberth et al., 1998; Xie, 2020), understanding the causes of this discrepancy is important (e.g., Lee et al., 2022; Scaife &

Smith, 2018; Watanabe et al., 2021; Wills et al., 2022). Another area where observations diverge from model predictions is the Southern Ocean. While models predict weak warming (see MMM in Figure 3), observations show a distinct cooling trend (Kang, Yu, et al., 2023). Many plausible drivers have been proposed to explain cooling of the Southern Ocean and its possible connection to the Tropical Eastern Pacific, but the relative contribution of different mechanisms is not fully understood (e.g., Dong et al., 2022, 2023; Ferreira et al., 2015; Hartmann, 2022; Hwang et al., 2017; Kang, Shin, et al., 2023; Latif et al., 2013; Luongo et al., 2023; Meehl et al., 2016; Roach et al., 2023; Schneider & Deser, 2018; J. H. L. Zhang et al., 2019, L. Zhang et al., 2019). At the same time, parts of the Arctic have been warming ∼7x faster than the global mean over 1980–2022, which may implicate the role of internally driven sea-ice decline associated with atmospheric circulation anomalies (e.g., Day et al., 2012; Ding et al., 2014; England et al., 2019; Isaksen et al., 2022; Roach & Blanchard-Wrigglesworth, 2022; Svendsen et al., 2021). Furthermore, many studies have indicated the potential connection between Arctic warming and Northern Hemisphere continental cooling and the role of internal variability (Blackport et al., 2019; Cohen et al., 2014; Fyfe, 2019; Kaufman et al., 2024; Palmer, 2014). Our study suggests that internal variability has made an important contribution to observed Arctic warming, Eastern Pacific cooling, and Southern Ocean cooling over 1980–2022.

Another notable result of this study is that the model-simulated internal SAT trend pattern associated with the i-GCAW has remarkable similarity to the inferred internal trend pattern by taking the difference between the observed SAT trend and the scaled MMM trend (c.f., Figures 2 and 3c). These features include many of the aforementioned discrepancies between observations and CMIP6 simulated warming, namely a warming of the Kara Sea concurrent with cooling of the Tropical Eastern Pacific and Southern Ocean. Importantly, all these features are agreed upon in sign by more than 80% of the simulations considered. This study is consistent with previous research that indicates that internal variability has a strong imprint in these regions individually (e.g., Watanabe et al., 2021; J. H. L. Zhang et al., 2019, L. Zhang et al., 2019) and that internal variability in these regions may even be linked via atmospheric and oceanic teleconnections (Ding et al., 2014; Dong et al., 2022; England et al., 2020). However, it is not necessary that all these features be connected through the same mode of internal variability (Feng et al., 2021), as features present in the i-GCAW may occur through separate modes of internal variability which might, by chance, occur simultaneously. Instead, results here suggest that these internally driven trend patterns are related to the rare manifestation of the i-GCAW, which is responsible for the inflation of AA over recent decades.

The spatial trend patterns associated with i-GCAW using different thresholds and the difference trend pattern (i.e., Figure 3c) are directly compared in Figure S5 in Supporting Information S1 using the same scale. While the spatial pattern associated with the i-GCAW (Figure 2) is consistent with the difference between observations and the forced response (Figure 3c), its magnitude is smaller, especially in the Tropical Eastern Pacific. This discrepancy may be due to biases in the forced response of climate models (e.g., Seager et al., 2019), biases in the historical forcing exerted to models (e.g., Fasullo et al., 2022), insufficient amplitude of multi-decadal internal variability in models (e.g., Laepple et al., 2023), other components of internal variability operating over 1980–2022 which are not captured by the i-GCAW composite, and/or biases in the observations (Karl et al., 2015). Here we note that compositing over the 25% of i-GCAW cases with the strongest cooling in the Tropical Eastern Pacific (Figure S5c in Supporting Information S1) can largely reconcile the magnitude of cooling in this region (Figure S5c vs. Figure S5d in Supporting Information S1), suggesting another possibility, that is, an extreme i-GCAW case might have occurred for 1980–2022. Figure S5 in Supporting Information S1 indicates that the difference between the observations and MMM trend patterns may be largely explained by internal variability.

This study does not preclude a role of biases in the forced response of models or errors in the historical forcings (Dong et al., 2022; Hwang et al., 2024; Tseng et al., 2023; Wills et al., 2022). If part of this discrepancy between Figures 2 and 3c (also see Figure S5 in Supporting Information S1) in the Tropical Eastern Pacific is caused by a bias in the modeled forced response, then this would suggest that the correction of forced response bias has a similar pattern to that of the internal variability in this region. This possibility might complicate efforts to separate forced and unforced climate variability, because many disentanglement techniques are dependent on pattern recognition methodologies (Po-Chedley et al., 2022; Wills et al., 2020). This possibility, however, would not affect our results because a forced response bias with an overestimation of warming in the Tropical Eastern Pacific but an underestimation of warming in the Arctic at the same time is very unlikely. As previously stated, it is also possible that models do not correctly represent the magnitude of internal variability at multi-decadal

timescales (Feng et al., 2021; Kravtsov et al., 2018; Laepple & Huybers, 2014; Laepple et al., 2023; Parsons et al., 2017; Rugenstein et al., 2023; Stout et al., 2023). Similarly, extreme events such as the 2022 heatwave in Antarctica continue to suggest that the observational record is too short in many instances to fully encapsulate the range of internal variability, and that models may not always simulate the full extent of real-world natural variability (Blanchard-Wrigglesworth et al., 2023; Lehner & Deser, 2023).

While more research is needed to fully attribute the causes of modeled-versus-observed differences in the pattern of SAT change, the identified pattern of internal variability and its similarity to features in the observational record suggests that the Earth did indeed experience an internally generated global cooling and Arctic warming pattern from 1980 to 2022. Quantifying the contribution of internal variability to differences in the simulated and observed pattern of SAT change is important because without knowing the relative contribution of internal variability versus biases in the simulated forced response, we are faced with significant uncertainties in decadal climate projections (Deser, 2020; Hu & Deser, 2013; Lehner et al., 2020; Wills et al., 2022). This study shows that the internal trend pattern associated with the i-GCAW can largely account for the discrepancy between observed and CMIP6 simulated patterns of warming from 1980 to 2022. Importantly, this internally generated trend pattern can be obtained by constraining simulations based only on their internally generated global cooling and Arctic warming and calls for further studies focused on this rare manifestation of internal variability.

Data Availability Statement

The data on which this article is based is the same as was used in S2023 (Sweeney, 2023).

Acknowledgments

This research was supported by the U.S. Department of Energy (DOE), Office of Science, Office of Biological and Environmental Research, Regional and Global Model Analysis (RGMA) program area, as part of the HiLAT-RASM project. This research was also supported by the NASA FINESST Grant 80NSSC22K1438 and NSF Grant AGS-2202812. Additional funding was provided by the Calvin Professorship in Atmospheric Sciences. S. P.-C. was supported through the PCMDI Project, which is funded by the RGMA program area of the Office of Science at DOE. M. Wang is funded with support of the Arctic Research Program of the NOAA Global Ocean Monitoring and Observing (GOMO) office through the Cooperative Institute for Climate, Ocean, and Ecosystem Studies (CICOES) under NOAA Cooperative Agreement NA20OAR4320271, Contribution No 2024-1337, and Pacific Marine Environmental Laboratory Contribution No 5599. Research at Lawrence Livermore National Laboratory was performed under the auspices of U.S. DOE Contract DE-AC52-07NA27344. The Pacific Northwest National Laboratory (PNNL) is operated for DOE by Battelle Memorial Institute under contract DE-AC05-76RLO1830. We would like to thank Prof. Yen-Ting Hwang for suggesting the use of CMIP6 piControl runs. We would also like to acknowledge high-performance computing support from Cheyenne (https://doi.org/10.5065/D6RX99HX) provided by NCAR's Computational and Information Systems Laboratory, sponsored by the National Science Foundation, for the analyses presented in this study and for data management, storage, and preservation.

References

Barnes, E. A., Hurrell, J. W., Ebert-Uphoff, I., Anderson, C., & Anderson, D. (2019). Viewing forced climate patterns through an AI lens. *Geophysical Research Letters*, *46*(22), 13389–13398. https://doi.org/10.1029/2019GL084944

Baxter, I., Ding, Q., Schweiger, A., L'Heureux, M., Baxter, S., Wang, T., et al. (2019). How tropical pacific surface cooling contributed to accelerated sea ice melt from 2007 to 2012 as ice is thinned by anthropogenic forcing. *Journal of Climate*, *32*(24), 8583–8602. https://doi.org/10.1175/JCLI-D-18-0783.1

Blackport, R., Screen, J. A., van der Wiel, K., & Bintanja, R. (2019). Minimal influence of reduced Arctic sea ice on coincident cold winters in mid-latitudes. *Nature Climate Change*, *9*(9), 697–704. https://doi.org/10.1038/s41558-019-0551-4

Blanchard-Wrigglesworth, E., Cox, T., Espinosa, Z. I., & Donohoe, A. (2023). The largest ever recorded heatwave—Characteristics and attribution of the antarctic heatwave of March 2022. *Geophysical Research Letters*, *50*(17), e2023GL104910. https://doi.org/10.1029/2023GL104910

Chylek, P., Folland, C., Klett, J. D., Wang, M., Hengartner, N., Lesins, G., & Dubey, M. K. (2022). Annual mean arctic amplification 1970–2020: Observed and simulated by CMIP6 climate models. *Geophysical Research Letters*, *49*(13), e2022GL099371. https://doi.org/10.1029/2022GL099371

Chylek, P., Folland, C. K., Klett, J. D., Wang, M., Lesins, G., & Dubey, M. K. (2023). High values of the arctic amplification in the early decades of the 21st century: Causes of discrepancy by CMIP6 models between observation and simulation. *Journal of Geophysical Research: Atmospheres*, *128*(23), e2023JD039269. https://doi.org/10.1029/2023JD039269

Chylek, P., Folland, C. K., Klett, J. D., Wang, M., Lesins, G., & Dubey, M. K. (2024). Why does the ensemble mean of CMIP6 models simulate arctic temperature more accurately than global temperature? *Atmosphere*, *15*(5), 567. https://doi.org/10.3390/atmos15050567

Cohen, J., Screen, J. A., Furtado, J. C., Barlow, M., Whittleston, D., Coumou, D., et al. (2014). Recent Arctic amplification and extreme mid-latitude weather. *Nature Geoscience*, *7*(9), 627–637. https://doi.org/10.1038/ngeo2234

Dai, A., Fyfe, J. C., Xie, S.-P., & Dai, X. (2015). Decadal modulation of global surface temperature by internal climate variability. *Nature Climate Change*, *5*(6), 555–559. https://doi.org/10.1038/nclimate2605

Day, J. J., Hargreaves, J. C., Annan, J. D., & Abe-Ouchi, A. (2012). Sources of multi-decadal variability in Arctic sea ice extent. *Environmental Research Letters*, *7*(3), 034011. https://doi.org/10.1088/1748-9326/7/3/034011

Deser, C. (2020). Certain uncertainty: The role of internal climate variability in projections of regional climate change and risk management. *Earth's Future*, *8*(12), e2020EF001854. https://doi.org/10.1029/2020EF001854

Deser, C., Knutti, R., Solomon, S., & Phillips, A. S. (2012). Communication of the role of natural variability in future North American climate. *Nature Climate Change*, *2*(11), 775–779. https://doi.org/10.1038/nclimate1562

Deser, C., Phillips, A., Bourdette, V., & Teng, H. (2012). Uncertainty in climate change projections: The role of internal variability. *Climate Dynamics*, *38*(3), 527–546. https://doi.org/10.1007/s00382-010-0977-x

Deser, C., Phillips, A. S., Alexander, M. A., & Smoliak, B. V. (2014). Projecting North American climate over the next 50 Years: Uncertainty due to internal variability. *Journal of Climate*, *27*(6), 2271–2296. https://doi.org/10.1175/JCLI-D-13-00451.1

Deser, C., Phillips, A. S., Simpson, I. R., Rosenbloom, N., Coleman, D., Lehner, F., et al. (2020). Isolating the evolving contributions of anthropogenic aerosols and greenhouse gases: A new CESM1 large ensemble community resource. *Journal of Climate*, *33*(18), 7835–7858. https://doi.org/10.1175/JCLI-D-20-0123.1

Ding, Q., Schweiger, A., L'Heureux, M., Steig, E. J., Battisti, D. S., Johnson, N. C., et al. (2019). Fingerprints of internal drivers of Arctic sea ice loss in observations and model simulations. *Nature Geoscience*, *12*(1), 28–33. https://doi.org/10.1038/s41561-018-0256-8

Ding, Q., & Steig, E. J. (2013). Temperature change on the antarctic peninsula linked to the tropical Pacific. *Journal of Climate*, *26*(19), 7570–7585. https://doi.org/10.1175/JCLI-D-12-00729.1

Ding, Q., Wallace, J. M., Battisti, D. S., Steig, E. J., Gallant, A. J. E., Kim, H.-J., & Geng, L. (2014). Tropical forcing of the recent rapid Arctic warming in northeastern Canada and Greenland. *Nature*, *509*(7499), 209–212. https://doi.org/10.1038/nature13260

Dong, Y., Pauling, A. G., Sadai, S., & Armour, K. C. (2022). Antarctic ice-sheet meltwater reduces transient warming and climate sensitivity through the sea-surface temperature pattern effect. *Geophysical Research Letters*, *49*(24), e2022GL101249. https://doi.org/10.1029/2022GL101249

Dong, Y., Polvani, L. M., & Bonan, D. B. (2023). Recent multi-decadal southern ocean surface cooling unlikely caused by southern annular mode trends. *Geophysical Research Letters*, *50*(23), e2023GL106142. https://doi.org/10.1029/2023GL106142

England, M., Jahn, A., & Polvani, L. (2019). Nonuniform contribution of internal variability to recent Arctic sea ice loss. *Journal of Climate*, *32*(13), 4039–4053. https://doi.org/10.1175/JCLI-D-18-0864.1

England, M. H., Kajtar, J. B., & Maher, N. (2015). Robust warming projections despite the recent hiatus. *Nature Climate Change*, *5*(5), 394–396. https://doi.org/10.1038/nclimate2575

England, M. R., Polvani, L. M., & Sun, L. (2020). Robust Arctic warming caused by projected Antarctic sea ice loss. *Environmental Research Letters*, *15*(10), 104005. https://doi.org/10.1088/1748-9326/abaada

Eyring, V., Bony, S., Meehl, G. A., Senior, C. A., Stevens, B., Stouffer, R. J., & Taylor, K. E. (2016). Overview of the Coupled Model Intercomparison Project Phase 6 (CMIP6) experimental design and organization. *Geoscientific Model Development*, *9*(5), 1937–1958. https://doi.org/10.5194/gmd-9-1937-2016

Fasullo, J. T., Golaz, J.-C., Caron, J. M., Rosenbloom, N., Meehl, G. A., Strand, W., et al. (2024). An overview of the E3SM version 2 large ensemble and comparison to other E3SM and CESM large ensembles. *Earth System Dynamics*, *15*(2), 367–386. https://doi.org/10.5194/esd-15-367-2024

Fasullo, J. T., Lamarque, J.-F., Hannay, C., Rosenbloom, N., Tilmes, S., DeRepentigny, P., et al. (2022). Spurious late historical-era warming in CESM2 driven by prescribed biomass burning emissions. *Geophysical Research Letters*, *49*(2), e2021GL097420. https://doi.org/10.1029/2021GL097420

Feng, X., Ding, Q., Wu, L., Jones, C., Baxter, I., Tardif, R., et al. (2021). A multidecadal-scale tropically driven global teleconnection over the past millennium and its recent strengthening. *Journal of Climate*, *34*(7), 2549–2565. https://doi.org/10.1175/JCLI-D-20-0216.1

Ferreira, D., Marshall, J., Bitz, C. M., Solomon, S., & Plumb, A. (2015). Antarctic ocean and sea ice response to ozone depletion: A two-time-scale problem. *Journal of Climate*, *28*(3), 1206–1226. https://doi.org/10.1175/JCLI-D-14-00313.1

Foster, G., & Rahmstorf, S. (2011). Global temperature evolution 1979–2010. *Environmental Research Letters*, *6*(4), 044022. https://doi.org/10.1088/1748-9326/6/4/044022

Fyfe, J. C. (2019). Midlatitudes unaffected by sea ice loss. *Nature Climate Change*, *9*(9), 649–650. https://doi.org/10.1038/s41558-019-0560-3

Gordon, E. M., Barnes, E. A., & Hurrell, J. W. (2021). Oceanic harbingers of pacific decadal oscillation predictability in CESM2 detected by neural networks. *Geophysical Research Letters*, *48*(21), e2021GL095392. https://doi.org/10.1029/2021GL095392

Hahn, L. C., Armour, K. C., Zelinka, M. D., Bitz, C. M., & Donohoe, A. (2021). Contributions to polar amplification in CMIP5 and CMIP6 models. *Frontiers in Earth Science*, *9*. https://doi.org/10.3389/feart.2021.710036

Hansen, J., Ruedy, R., Sato, M., & Lo, K. (2010). Global surface temperature change. *Reviews of Geophysics*, *48*(4), RG4004. https://doi.org/10.1029/2010RG000345

Hartmann, D. L. (2022). The Antarctic ozone hole and the pattern effect on climate sensitivity. *Proceedings of the National Academy of Sciences of the United States of America*, *119*(35), e2207889119. https://doi.org/10.1073/pnas.2207889119

Hu, A., & Deser, C. (2013). Uncertainty in future regional sea level rise due to internal climate variability. *Geophysical Research Letters*, *40*(11), 2768–2772. https://doi.org/10.1002/grl.50531

Hwang, Y.-T., Xie, S.-P., Chen, P.-J., Tseng, H.-Y., & Deser, C. (2024). Contribution of anthropogenic aerosols to persistent La Niña-like conditions in the early 21st century. *Proceedings of the National Academy of Sciences of the United States of America*, *121*(5), e2315124121. https://doi.org/10.1073/pnas.2315124121

Hwang, Y.-T., Xie, S.-P., Deser, C., & Kang, S. M. (2017). Connecting tropical climate change with Southern Ocean heat uptake. *Geophysical Research Letters*, *44*(18), 9449–9457. https://doi.org/10.1002/2017GL074972

Intergovernmental Panel on Climate Change (IPCC). (2023). Future global climate: Scenario-based projections and near-term information. In *Climate change 2021 – The physical science basis: Working group I contribution to the sixth assessment report of the intergovernmental panel on climate change* (pp. 553–672). Cambridge University Press. https://doi.org/10.1017/9781009157896.006

Isaksen, K., Nordli, Ø., Ivanov, B., Køltzow, M. A. Ø., Aaboe, S., Gjelten, H. M., et al. (2022). Exceptional warming over the Barents area. *Scientific Reports*, *12*(1), 9371. https://doi.org/10.1038/s41598-022-13568-5

Kang, S. M., Shin, Y., Kim, H., Xie, S.-P., & Hu, S. (2023). Disentangling the mechanisms of equatorial Pacific climate change. *Science Advances*, *9*(19), eadf5059. https://doi.org/10.1126/sciadv.adf5059

Kang, S. M., Yu, Y., Deser, C., Zhang, X., Kang, I.-S., Lee, S.-S., et al. (2023). Global impacts of recent Southern Ocean cooling. *Proceedings of the National Academy of Sciences of the United States of America*, *120*(30), e2300881120. https://doi.org/10.1073/pnas.2300881120

Karl, T. R., Arguez, A., Huang, B., Lawrimore, J. H., McMahon, J. R., Menne, M. J., et al. (2015). Possible artifacts of data biases in the recent global surface warming hiatus. *Science*, *348*, 1469–1472. https://doi.org/10.1126/science.aaa5632

Kaufman, Z., Feldl, N., & Beaulieu, C. (2024). Warm Arctic–Cold Eurasia pattern driven by atmospheric blocking in models and observations. *Environmental Research: Climate*, *3*(1), 015006. https://doi.org/10.1088/2752-5295/ad1f40

Kay, J. E., Deser, C., Phillips, A., Mai, A., Hannay, C., Strand, G., et al. (2015). The Community Earth System Model (CESM) large ensemble project: A community resource for studying climate change in the presence of internal climate variability. *Bulletin of the American Meteorological Society*, *96*(8), 1333–1349. https://doi.org/10.1175/BAMS-D-13-00255.1

Kay, J. E., Holland, M. M., & Jahn, A. (2011). Inter-annual to multi-decadal Arctic sea ice extent trends in a warming world. *Geophysical Research Letters*, *38*(15), L15708. https://doi.org/10.1029/2011GL048008

Kosaka, Y., & Xie, S.-P. (2013). Recent global-warming hiatus tied to equatorial Pacific surface cooling. *Nature*, *501*(7467), 403–407. https://doi.org/10.1038/nature12534

Kravtsov, S., Grimm, C., & Gu, S. (2018). Global-scale multidecadal variability missing in state-of-the-art climate models. *Npj Climate and Atmospheric Science*, *1*(1), 1–10. https://doi.org/10.1038/s41612-018-0044-6

Labe, Z. M., & Barnes, E. A. (2022). Predicting slowdowns in decadal climate warming trends with explainable neural networks. *Geophysical Research Letters*, *49*(9), e2022GL098173. https://doi.org/10.1029/2022GL098173

Laepple, T., & Huybers, P. (2014). Global and regional variability in marine surface temperatures. *Geophysical Research Letters*, *41*(7), 2528–2534. https://doi.org/10.1002/2014GL059345

Laepple, T., Ziegler, E., Weitzel, N., Hébert, R., Ellerhoff, B., Schoch, P., et al. (2023). Regional but not global temperature variability underestimated by climate models at supradecadal timescales. *Nature Geoscience*, *16*(11), 958–966. https://doi.org/10.1038/s41561-023-01299-9

Latif, M., Martin, T., & Park, W. (2013). Southern ocean sector centennial climate variability and recent decadal trends. *Journal of Climate*, *26*(19), 7767–7782. https://doi.org/10.1175/JCLI-D-12-00281.1

Lee, S., L'Heureux, M., Wittenberg, A. T., Seager, R., O'Gorman, P. A., & Johnson, N. C. (2022). On the future zonal contrasts of equatorial Pacific climate: Perspectives from observations, simulations, and theories. *Npj Climate and Atmospheric Science*, *5*(1), 1–15. https://doi.org/10.1038/s41612-022-00301-2

Lehner, F., & Deser, C. (2023). Origin, importance, and predictive limits of internal climate variability. *Environmental Research: Climate*, *2*(2), 023001. https://doi.org/10.1088/2752-5295/accf30

Lehner, F., Deser, C., Maher, N., Marotzke, J., Fischer, E. M., Brunner, L., et al. (2020). Partitioning climate projection uncertainty with multiple large ensembles and CMIP5/6. *Earth System Dynamics*, *11*(2), 491–508. https://doi.org/10.5194/esd-11-491-2020

Lenssen, N. J. L., Schmidt, G. A., Hansen, J. E., Menne, M. J., Persin, A., Ruedy, R., & Zyss, D. (2019). Improvements in the GISTEMP uncertainty model. *Journal of Geophysical Research: Atmospheres*, *124*(12), 6307–6326. https://doi.org/10.1029/2018JD029522

Luongo, M. T., Xie, S.-P., Eisenman, I., Hwang, Y.-T., & Tseng, H.-Y. (2023). A pathway for Northern Hemisphere extratropical cooling to elicit a tropical response. *Geophysical Research Letters*, *50*(2), e2022GL100719. https://doi.org/10.1029/2022GL100719

Manabe, S., & Wetherald, R. T. (1975). The effects of doubling the CO_2 concentration on the climate of a general circulation model. *Journal of the Atmospheric Sciences*, *32*(1), 3–15. https://doi.org/10.1175/1520-0469(1975)032<0003:TEODTC>2.0.CO;2

Meehl, G. A., Arblaster, J. M., Bitz, C. M., Chung, C. T. Y., & Teng, H. (2016). Antarctic sea-ice expansion between 2000 and 2014 driven by tropical Pacific decadal climate variability. *Nature Geoscience*, *9*(8), 590–595. https://doi.org/10.1038/ngeo2751

Morice, C. P., Kennedy, J. J., Rayner, N. A., Winn, J. P., Hogan, E., Killick, R. E., et al. (2021). An updated assessment of near-surface temperature change from 1850: The HadCRUT5 data set. *Journal of Geophysical Research: Atmospheres*, *126*(3), e2019JD032361. https://doi.org/10.1029/2019JD032361

O'Neill, B. C., Tebaldi, C., van Vuuren, D. P., Eyring, V., Friedlingstein, P., Hurtt, G., et al. (2016). The Scenario Model Intercomparison Project (ScenarioMIP) for CMIP6. *Geoscientific Model Development*, *9*(9), 3461–3482. https://doi.org/10.5194/gmd-9-3461-2016

Palmer, T. (2014). Record-breaking winters and global climate change. *Science*, *344*(6186), 803–804. https://doi.org/10.1126/science.1255147

Parsons, L. A., Loope, G. R., Overpeck, J. T., Ault, T. R., Stouffer, R., & Cole, J. E. (2017). Temperature and precipitation variance in CMIP5 simulations and paleoclimate records of the last millennium. *Journal of Climate*, *30*(22), 8885–8912. https://doi.org/10.1175/JCLI-D-16-0863.1

Po-Chedley, S., Fasullo, J. T., Siler, N., Labe, Z. M., Barnes, E. A., Bonfils, C. J. W., & Santer, B. D. (2022). Internal variability and forcing influence model–satellite differences in the rate of tropical tropospheric warming. *Proceedings of the National Academy of Sciences of the United States of America*, *119*(47), e2209431119. https://doi.org/10.1073/pnas.2209431119

Po-Chedley, S., Santer, B. D., Fueglistaler, S., Zelinka, M. D., Cameron-Smith, P. J., Painter, J. F., & Fu, Q. (2021). Natural variability contributes to model–satellite differences in tropical tropospheric warming. *Proceedings of the National Academy of Sciences of the United States of America*, *118*(13), e2020962118. https://doi.org/10.1073/pnas.2020962118

Rader, J. K., Barnes, E. A., Ebert-Uphoff, I., & Anderson, C. (2022). Detection of forced change within combined climate fields using explainable neural networks. *Journal of Advances in Modeling Earth Systems*, *14*(7), e2021MS002941. https://doi.org/10.1029/2021MS002941

Räisänen, J. (2021). Effect of atmospheric circulation on surface air temperature trends in years 1979–2018. *Climate Dynamics*, *56*(7), 2303–2320. https://doi.org/10.1007/s00382-020-05590-y

Rantanen, M., Karpechko, A. Y., Lipponen, A., Nordling, K., Hyvärinen, O., Ruosteenoja, K., et al. (2022). The Arctic has warmed nearly four times faster than the globe since 1979. *Communications Earth & Environment*, *3*(1), 1–10. https://doi.org/10.1038/s43247-022-00498-3

Roach, L. A., & Blanchard-Wrigglesworth, E. (2022). Observed winds crucial for September Arctic sea ice loss. *Geophysical Research Letters*, *49*(6), e2022GL097884. https://doi.org/10.1029/2022GL097884

Roach, L. A., Mankoff, K. D., Romanou, A., Blanchard-Wrigglesworth, E., Haine, T. W. N., & Schmidt, G. A. (2023). Winds and meltwater together lead to southern ocean surface cooling and sea ice expansion. *Geophysical Research Letters*, *50*(24), e2023GL105948. https://doi.org/10.1029/2023GL105948

Rodgers, K. B., Lee, S.-S., Rosenbloom, N., Timmermann, A., Danabasoglu, G., Deser, C., et al. (2021). Ubiquity of human-induced changes in climate variability. *Earth System Dynamics*, *12*(4), 1393–1411. https://doi.org/10.5194/esd-12-1393-2021

Rohde, R. A., & Hausfather, Z. (2020). The Berkeley Earth land/ocean temperature record. *Earth System Science Data*, *12*(4), 3469–3479. https://doi.org/10.5194/essd-12-3469-2020

Rosenblum, E., & Eisenman, I. (2017). Sea ice trends in climate models only accurate in runs with biased global warming. *Journal of Climate*, *30*(16), 6265–6278. https://doi.org/10.1175/JCLI-D-16-0455.1

Rugenstein, M., Dhame, S., Olonscheck, D., Wills, R. J., Watanabe, M., & Seager, R. (2023). Connecting the SST pattern problem and the hot model problem. *Geophysical Research Letters*, *50*(22), e2023GL105488. https://doi.org/10.1029/2023GL105488

Scaife, A. A., & Smith, D. (2018). A signal-to-noise paradox in climate science. *Npj Climate and Atmospheric Science*, *1*(1), 1–8. https://doi.org/10.1038/s41612-018-0038-4

Schlesinger, M. E., & Ramankutty, N. (1994). An oscillation in the global climate system of period 65–70 years. *Nature*, *367*(6465), 723–726. https://doi.org/10.1038/367723a0

Schneider, D. P., & Deser, C. (2018). Tropically driven and externally forced patterns of Antarctic sea ice change: Reconciling observed and modeled trends. *Climate Dynamics*, *50*(11), 4599–4618. https://doi.org/10.1007/s00382-017-3893-5

Screen, J. A., & Deser, C. (2019). Pacific Ocean variability influences the time of emergence of a seasonally ice-free arctic ocean. *Geophysical Research Letters*, *46*(4), 2222–2231. https://doi.org/10.1029/2018GL081393

Seager, R., Cane, M., Henderson, N., Lee, D.-E., Abernathey, R., & Zhang, H. (2019). Strengthening tropical Pacific zonal sea surface temperature gradient consistent with rising greenhouse gases. *Nature Climate Change*, *9*(7), 517–522. https://doi.org/10.1038/s41558-019-0505-x

Seager, R., Henderson, N., & Cane, M. (2022). Persistent discrepancies between observed and modeled trends in the tropical Pacific Ocean. *Journal of Climate*, *35*(14), 4571–4584. https://doi.org/10.1175/JCLI-D-21-0648.1

Sippel, S., Meinshausen, N., Székely, E., Fischer, E., Pendergrass, A. G., Lehner, F., & Knutti, R. (2021). Robust detection of forced warming in the presence of potentially large climate variability. *Science Advances*, *7*, eabh4429. https://doi.org/10.1126/sciadv.abh4429

Stout, R. C., Proistosescu, C., & Roe, G. (2023). Fingerprinting low-frequency last millennium temperature variability in forced and unforced climate models. *Journal of Climate*, *36*(20), 7005–7023. https://doi.org/10.1175/JCLI-D-22-0810.1

Stuecker, M. F., Bitz, C. M., & Armour, K. C. (2017). Conditions leading to the unprecedented low Antarctic sea ice extent during the 2016 austral spring season. *Geophysical Research Letters*, *44*(17), 9008–9019. https://doi.org/10.1002/2017GL074691

Svendsen, L., Keenlyside, N., Muilwijk, M., Bethke, I., Omrani, N.-E., & Gao, Y. (2021). Pacific contribution to decadal surface temperature trends in the Arctic during the twentieth century. *Climate Dynamics*, *57*(11), 3223–3243. https://doi.org/10.1007/s00382-021-05868-9

Sweeney, A. (2023). Data for internal variability increased arctic amplification from 1980-2022 [Dataset]. *Zenodo*. https://doi.org/10.5281/zenodo.8286633

Sweeney, A. J., Fu, Q., Po-Chedley, S., Wang, H., & Wang, M. (2023). Internal variability increased arctic amplification during 1980–2022. *Geophysical Research Letters*, *50*(24), e2023GL106060. https://doi.org/10.1029/2023GL106060

Tokarska, K. B., Stolpe, M. B., Sippel, S., Fischer, E. M., Smith, C. J., Lehner, F., & Knutti, R. (2020). Past warming trend constrains future warming in CMIP6 models. *Science Advances*, *6*(12), eaaz9549. https://doi.org/10.1126/sciadv.aaz9549

Trenberth, K. E., Branstator, G. W., Karoly, D., Kumar, A., Lau, N.-C., & Ropelewski, C. (1998). Progress during TOGA in understanding and modeling global teleconnections associated with tropical sea surface temperatures. *Journal of Geophysical Research*, *103*(C7), 14291–14324. https://doi.org/10.1029/97JC01444

Tseng, H.-Y., Hwang, Y.-T., Xie, S.-P., Tseng, Y.-H., Kang, S. M., Luongo, M. T., & Eisenman, I. (2023). Fast and slow responses of the tropical pacific to radiative forcing in northern high latitudes. *Journal of Climate*, *36*(16), 5337–5349. https://doi.org/10.1175/JCLI-D-22-0622.1

Wallace, J. M., Fu, Q., Smoliak, B. V., Lin, P., & Johanson, C. M. (2012). Simulated versus observed patterns of warming over the extratropical Northern Hemisphere continents during the cold season. *Proceedings of the National Academy of Sciences of the United States of America*, *109*(36), 14337–14342. https://doi.org/10.1073/pnas.1204875109

Watanabe, M., Dufresne, J.-L., Kosaka, Y., Mauritsen, T., & Tatebe, H. (2021). Enhanced warming constrained by past trends in equatorial Pacific sea surface temperature gradient. *Nature Climate Change*, *11*(1), 33–37. https://doi.org/10.1038/s41558-020-00933-3

Wills, R. C. J., Battisti, D. S., Armour, K. C., Schneider, T., & Deser, C. (2020). Pattern recognition methods to separate forced responses from internal variability in climate model ensembles and observations. *Journal of Climate*, *33*(20), 8693–8719. https://doi.org/10.1175/JCLI-D-19-0855.1

Wills, R. C. J., Dong, Y., Proistosecu, C., Armour, K. C., & Battisti, D. S. (2022). Systematic climate model biases in the large-scale patterns of recent sea-surface temperature and sea-level pressure change. *Geophysical Research Letters*, *49*(17), e2022GL100011. https://doi.org/10.1029/2022GL100011

Xie, S.-P. (2020). Ocean warming pattern effect on global and regional climate change. *AGU Advances*, *1*(1), e2019AV000130. https://doi.org/10.1029/2019AV000130

Xie, S.-P., & Kosaka, Y. (2017). What caused the global surface warming Hiatus of 1998–2013? *Current Climate Change Reports*, *3*(2), 128–140. https://doi.org/10.1007/s40641-017-0063-0

Ye, K., & Messori, G. (2021). Inter-model spread in the wintertime Arctic amplification in the CMIP6 models and the important role of internal climate variability. *Global and Planetary Change*, *204*, 103543. https://doi.org/10.1016/j.gloplacha.2021.103543

Zhang, J. H. L., Huang, B., Menne, M. J., Yin, X., Sánchez-Lugo, A., Gleason, B. E., et al. (2019a). Updated temperature data give a sharper view of climate trends. Retrieved from http://eos.org/science-updates/updated-temperature-data-give-a-sharper-view-of-climate-trends

Zhang, L., Delworth, T. L., Cooke, W., & Yang, X. (2019b). Natural variability of Southern Ocean convection as a driver of observed climate trends. *Nature Climate Change*, *9*(1), 59–65. https://doi.org/10.1038/s41558-018-0350-3

Zhou, W., Leung, L. R., & Lu, J. (2024). Steady threefold Arctic amplification of externally forced warming masked by natural variability. *Nature Geoscience*. https://doi.org/10.1038/s41561-024-01441-1

Geophysical Research Letters

Supporting Information for

Unique Temperature Trend Pattern Associated with Internally Driven Arctic Warming and Global Cooling during 1980-2022

Aodhan J. Sweeney[1], Qiang Fu[1], Stephen Po-Chedley[2], Hailong Wang[3], Muyin Wang[4,5]

[1]University of Washington, Department of Atmospheric Sciences
[2]Program for Climate Model Diagnosis and Intercomparison, Lawrence Livermore National Laboratory, Livermore, CA, USA
[3]Atmospheric Sciences and Global Change Division, PNNL
[4]Pacific Marine Environmental Laboratory, Oceanic and Atmospheric Research, NOAA
[5]University of Washington, Cooperative Institute for Climate, Ocean, and Ecosystem Studies

Contents of this file

Introduction

Table S1 is referenced in the main text. Supplementary figures (Figures S1 to S7) are also referenced throughout the main text.

Table S1: Large ensembles used for analysis. Time period refers to the years of data used for the analysis. *N trend maps* is the total number of 43-year trend maps from each model. It is calculated by taking the total number of 43-year trends (e.g., from 1850-2050 for CESM2 this would be 31) and multiplying this by the total number of ensemble members (e.g., for CESM2 this would be 50). *N i-GCAW* is the number of times for which a given model produces internally generated global-cooling and Arctic-warming greater than $\frac{\sigma_{Global}}{2}$ and $\frac{\sigma_{Arctic}}{2}$ respectively (see text for details). i-*GCAW Frequency* shows the percentage of 43-year trend maps produced by the model that fall into this i-GCAW category.

Model	Time Period	N Trend maps (n ensembles)	N i-GCAW	Frequency i-GCAW
CESM2-SBMB	1850-2047	1550 (50)	32	2.1%
MPI-ESM1-2-LR	1850-2047	310 (10)	1	0.3%
MIROC6	1850-2047	1550 (50)	11	0.7%
CESM2	1850-2047	1550 (50)	28	1.8%
ACCESS-ESM1-5	1850-2047	930 (30)	11	1.2%
IPSL-CM6A-LR	1850-2047	341 (11)	4	1.2%
CanESM5	1850-2047	775 (25)	22	2.8%
E3SM-V2-0	1850-2047	651 (21)	18	2.8%
MPI-ESM1-2-HR	1850-2014	240 (10)	1	0.4%
GISS-E2-1-H	1850-2014	240 (10)	7	2.9%
NorCPM1	1850-2014	696 (29)	12	1.7%
GISS-E2-1-G	1850-2014	288 (12)	7	2.4%

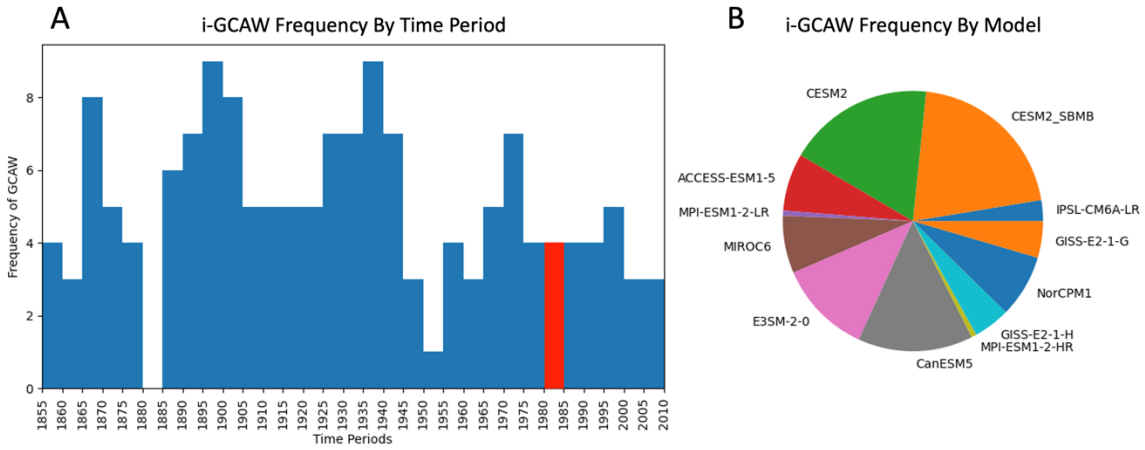

Fig. S1: (A) The number of the i-GCAW as a function of starting time for the 43-year trends from all large ensembles. Red bar highlights the 1980-2022 period. (B) Relative model contributions of all the 154 i-GCAW patterns found in the main text.

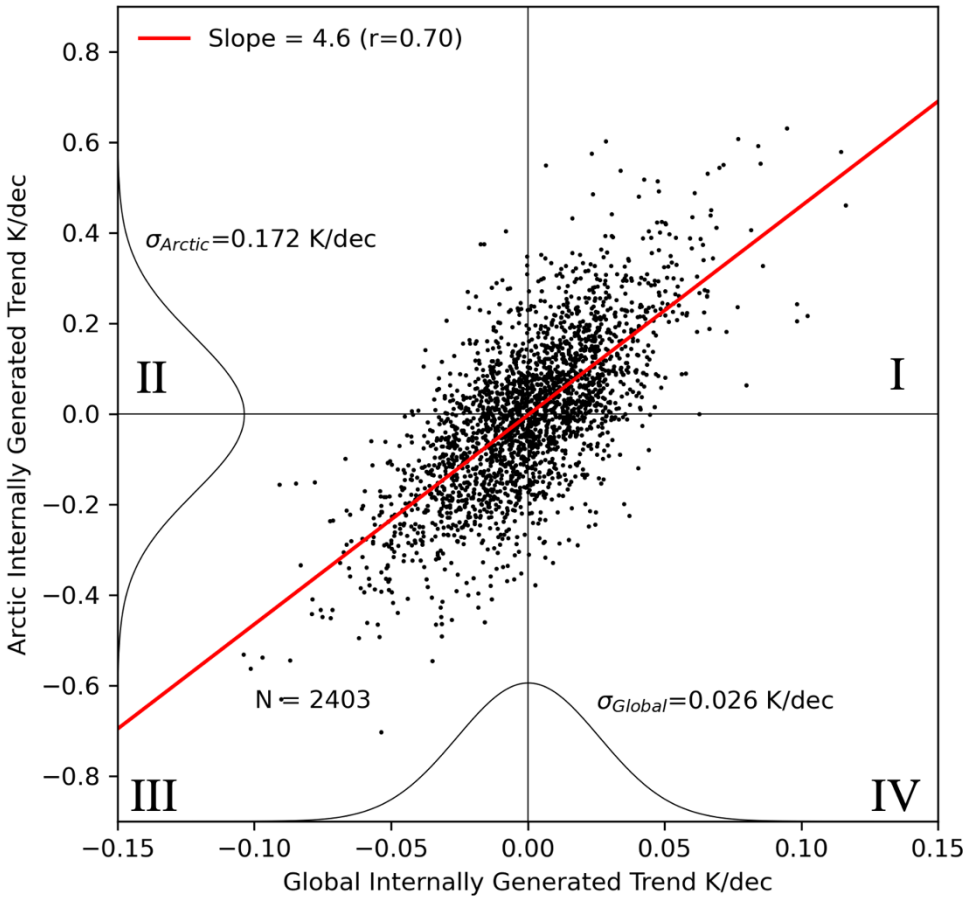

Fig. S2: The same as Fig. 1 but using CMIP6 Pre-Industrial (pi) Control runs. Models chosen for composite have at least 100 years of data, including CESM2, GISS-E2-1-G, GISS-E2-1-H, CanESM5, ACCESS-ESM1-5, MIROC6, IPSL-CM6A-LR, MPI-ESM1-2-LR, MPI-ESM1-2-HR, and NorCPM1. The i-GCAW pattern occurs in 1.4% of the total piControl simulated 43-year period samples (33 of 2403)

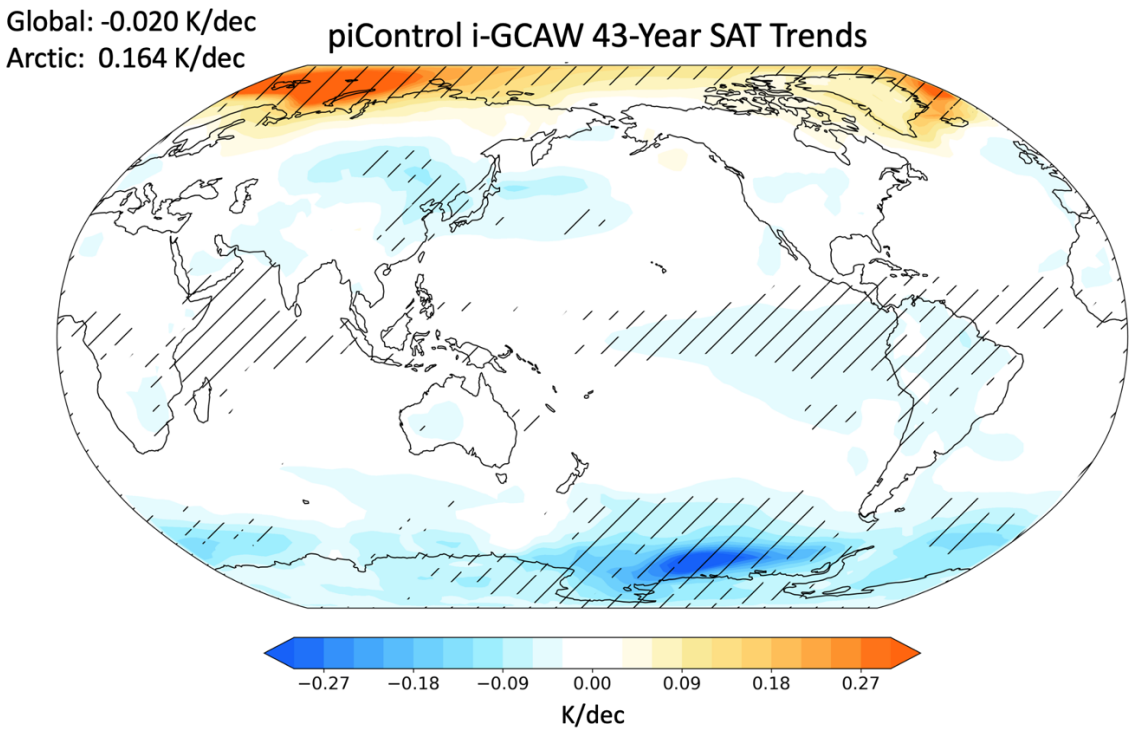

Fig S3: The same as Fig. 2 but using CMIP6 Pre-Industrial (Pi) Control runs.

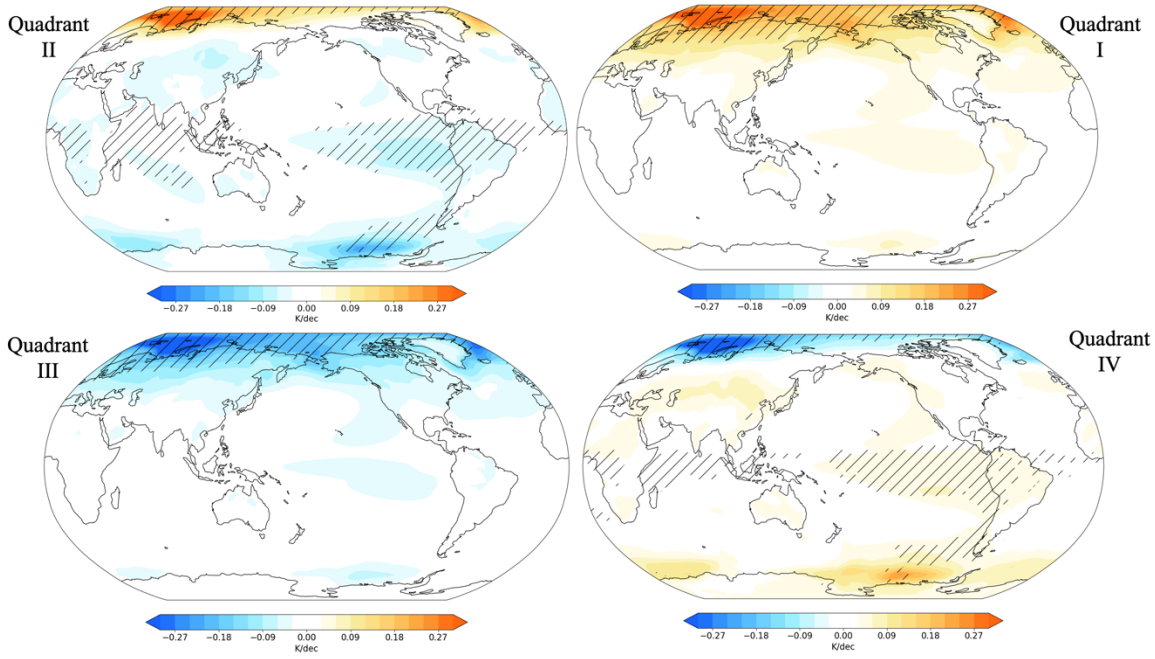

Fig. S4: Comparison of SAT internal trend patterns from each of the four quadrants shown in Fig. 1 of the main text. Each map is found by taking averaging over the simulations which have global and Arctic internal variability trend magnitudes larger than $\frac{\sigma_{Global}}{2}$ and $\frac{\sigma_{Arctic}}{2}$, respectively.

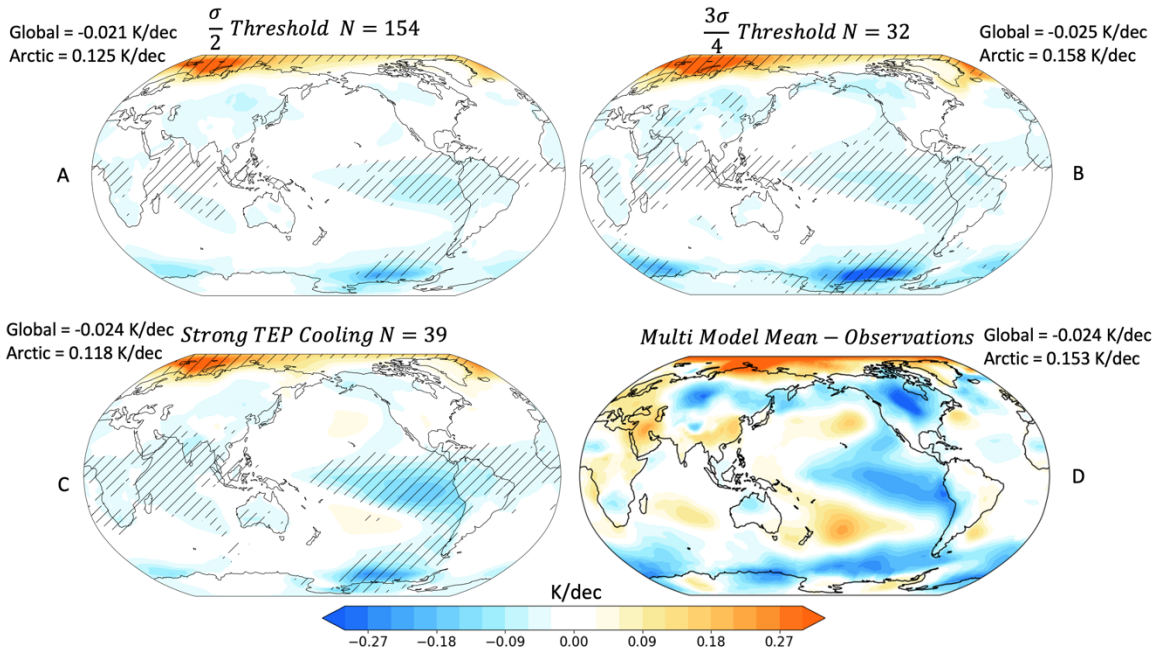

Fig. S5: Comparison of the internal trend pattern associated with the i-GCAW from Fig. 2 (A) with that using the more stringent criterion of global and Arctic internal variability trend magnitudes stronger than $\frac{3}{4}\sigma_{Global}$ and $\frac{3}{4}\sigma_{Arctic}$, respectively (B). Note that using this more stringent criterion reduces the number of samples to 32 from 154 when using the $\frac{1}{2}\sigma_{Global}$ and $\frac{1}{2}\sigma_{Arctic}$ criterion. The pattern associated with the i-GCAW cases using only the strongest 25% of Tropical Eastern Pacific cooling is also shown (C). The difference pattern between observations and the scaled MMM shown in Fig. 3C of the main text is included (D) using a common color bar scale for a comparison.

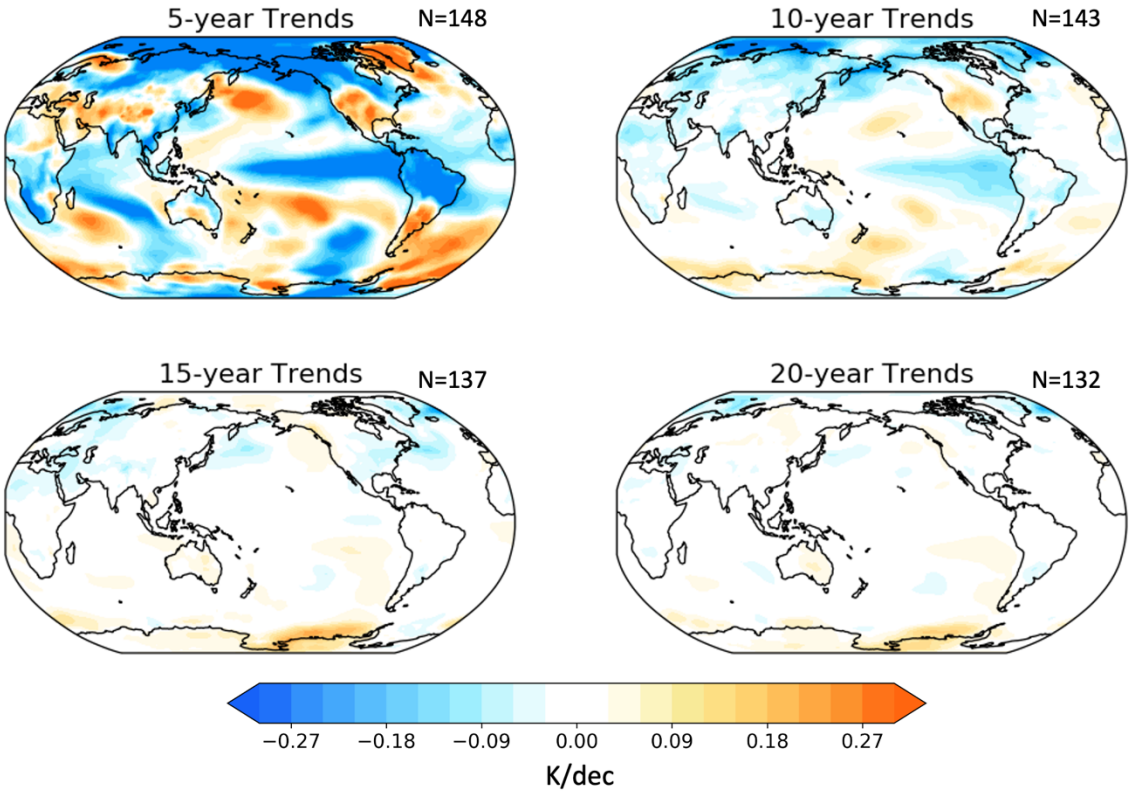

Fig. S6: 5-, 10-, 15-, and 20-year SAT trend patterns following identification of an i-GCAW. None of the trends show 80% agreement in sign between different trajectories (i.e., no hatching on any plot). The number of samples used for each composite (N) is shown for each trend map.

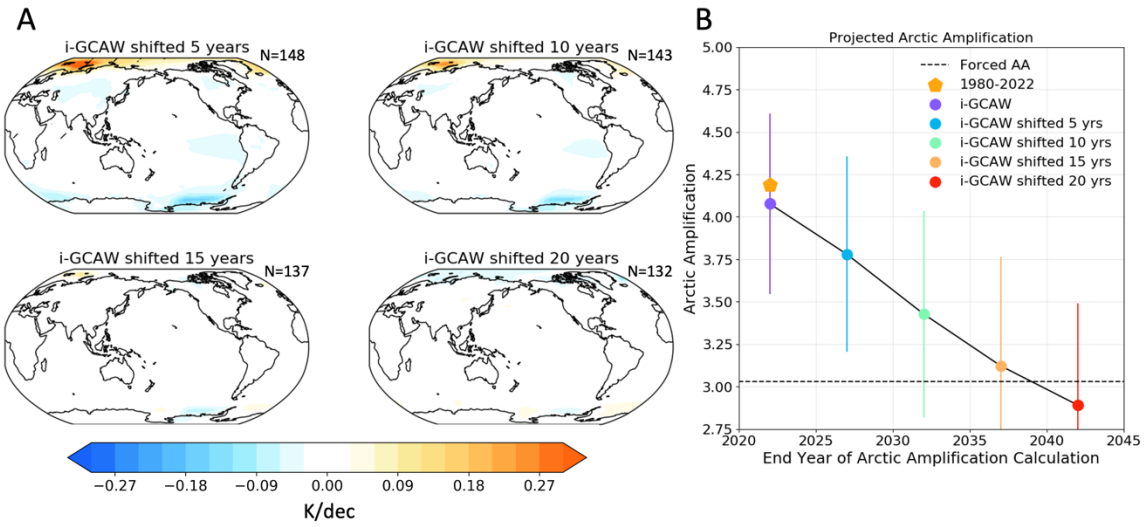

Fig. S7: A recreation of Figure 4 from the main text using 43-year trends based on the trajectory analysis. Panel A shows 43-year trends of multidecadal variability shifted by 5, 10, 15, and 20 years. The number of samples used for the composite (N) is shown for each trend map. Panel B shows the implications of these different configurations of internal variability on Arctic Amplification. The horizontal dashed line shows the 1980-2022 estimated forced trend from Sweeney et al. (2023).